Spatial distributions of the ion to electron temperature ratio in the magnetosheath and plasma sheet

Chih-Ping Wang,[1] Matina Gkioulidou,[1,2] Larry R. Lyons,[1] and Vassilis Angelopoulos[3]

Received 24 February 2012; revised 25 June 2012; accepted 27 June 2012; published 10 August 2012.

[1] We have used THEMIS measurements to determine how the ion and electron temperatures and their ratio (T_i/T_e) change spatially in the magnetosheath and plasma sheet and to identify the processes responsible for the variations. Magnetosheath T_i/T_e varies from ~4–12 with higher ratios observed during larger solar wind speed and at locations closer to the magnetopause. T_i/T_e remains almost unchanged as particles flow downstream and cool adiabatically. Across the flank magnetopause from the magnetosheath to a plasma sheet that is cool with abundant cold plasma, temperature and specific entropy for ions and electrons increase significantly while T_i/T_e remains similar, indicating that the magnetosheath ions and electrons are non-adiabatically energized with similar proportion while entering the magnetosphere. Within the tail plasma sheet, T_i/T_e varies from ~6 to 10 when plasma is relatively cool to ~2 to 5 when relatively warm. With this correlation, T_i/T_e is higher closer to the flanks and during northward interplanetary magnetic field (IMF), while lower T_i/T_e is more often seen during higher AE around midnight. The distinguishably lower T_i/T_e for warmer plasma in the near-Earth plasma sheet is likely due to additional non-adiabatic heating of electrons more than ions as particles move earthward and are adiabatically energized. As particles move into the near-Earth magnetosphere, strengthening magnetic drift brings more hotter ions toward dusk and more hotter electrons toward dawn, resulting in a strong T_i/T_e dawn-dusk asymmetry with very high T_i/T_e (~15 to 100) near dusk and very low T_i/T_e (~1) near dawn.

Citation: Wang, C.-P., M. Gkioulidou, L. R. Lyons, and V. Angelopoulos (2012), Spatial distributions of the ion to electron temperature ratio in the magnetosheath and plasma sheet, *J. Geophys. Res.*, *117*, A08215, doi:10.1029/2012JA017658.

1. Introduction

[2] Temperature of ions and electrons changes as these particles move from the solar wind to the magnetosheath and then to the magnetosphere. The temperature change can be due to various processes. Some of the processes directly change particle energy, such as adiabatic heating or cooling, or non-adiabatic heating through reconnection or wave-particle interaction. Some processes alter temperature because of adding or subtracting particles of a certain energy range from a population, such as local sources or losses or energy-dependent magnetic drift. There can be more than one process working on particles of the same species at the same time. The dominant processes for ions and electrons can also be different. If a process changes ion and electron temperature equally, then the ratio of ion temperature (T_i) to electron temperature (T_e) will remain constant as temperature changes. Variation of the temperature ratio (T_i/T_e) is an indicator of the difference in the temperature changes between ions and electrons, and is thus important for understanding the underlying processes.

[3] T_i/T_e has been investigated in different space regions using observations from different satellites. In the magnetosheath, statistically studies [*Paschmann et al.*, 1993; *Phan et al.*, 1994] show that T_i/T_e is ~6 to 12 at the dayside magnetosheath. A much lower T_i/T_e (~3) is reported in an event study at the flank magnetosheath near dusk during low solar wind Mach number [*Lavraud et al.*, 2009]. Inside the magnetosphere, T_i/T_e in the near-Earth plasma sheet ($X > -30\ R_E$) is found to be ~6–8 from the statistical analysis of AMPTE/IRM [*Baumjohann et al.* 1989, 1993] and Geotail data [*Kaufmann et al.*, 2005], while a statistical study with the Cluster observations shows a lower $T_i/T_e \sim 3.5$ [*Artemyev et al.*, 2011]. In the distant tail ($X < -30\ R_E$), T_i/T_e varies from 4.8 to 7.8 [*Slavin et al.*, 1985; *Paterson and Frank*, 1994]. While that the above statistical averages do not seem too different from one region to another, variations within each region are large. For example, in the magnetosheath T_i/T_e can vary from ~5 to 18 [*Phan et al.*, 1994]. It is still not fully clear whether these variations are due to spatial variations (most of the above studies did not provide spatial distributions likely due to limited data number and coverage) or/and are associated with external or internal factors and processes, such as changes in the solar wind

[1]Department of Atmospheric and Oceanic Sciences, University of California, Los Angeles, California, USA.
[2]Now at Johns Hopkins University Applied Physics Laboratory, Laurel, Maryland, USA.
[3]Department of Earth and Space Sciences, University of California, Los Angeles, California, USA.

Corresponding author: C.-P. Wang, Department of Atmospheric and Oceanic Sciences, University of California, 405 Hilgard Ave., PO Box 951565, Los Angeles, CA 90095, USA. (cat@atmos.ucla.edu)

0148-0227/12/2012JA017658

conditions or changes in dominant energization processes. Determining how T_i/T_e changes spatially in the magnetosheath and magnetosphere is crucial to identify the external and internal processes responsible for the variations.

[4] In this study, we used THEMIS measurements to statistically determine the spatial distributions of T_i/T_e in the magnetosheath and plasma sheet from X = 20 to −60 R_E. As described in Section 2, THEMIS has measured plasma in the magnetosheath and magnetosphere at low latitudes since 2007, providing sufficient data coverage for establishing spatial distributions with good spatial resolution. In addition, the wide energy range covered by the THEMIS detectors allows us to obtain temperature measurements and thus the temperature ratio more accurately than the previous studies. In Section 3, we investigate and discuss the change of T_i/T_e in the magnetosheath with increasing distance from the subsolar point as well as away from the magnetopause, and its correlation with the solar wind speed. Moving into the magnetosphere, we show how T_i/T_e in the plasma sheet varies radially from the distant tail to the near-Earth magnetosphere as well as across the tail from the flanks to midnight. We determine and identify the causes for the correlation of plasma sheet T_i/T_e with ion temperature, solar wind speed, interplanetary magnetic field (IMF), and the AE level. We also examine changes in ion and electron specific entropy in the magnetosheath and plasma sheet to determine if the temperature change is due to an adiabatic process. We further compare an observed MLT asymmetry of T_i/T_e in the near-Earth magnetosphere with the simulation results of the Rice Convection Model to explain the strong dawn-dusk asymmetry.

2. Data Selection

[5] In this study, the ion and electron temperatures in the magnetosheath and magnetosphere are obtained from the THEMIS spacecraft while those in the solar wind are from the Wind spacecraft. Temperature is computed from the measured particle distributions, $T = (m/3k_B n) \int (v-v_b)(v-v_b) f(v) d^3v$, where m is the particle mass, n is number density, v is particle velocity, v_b is the bulk flow velocity, and f is the phase space density. Note that temperature calculated this way for any type of distribution function is called kinetic temperature and is not necessarily a temperature in the thermodynamic sense, which can only be calculated for plasma in thermal equilibrium [*Baumjohann and Treumann*, 1996]. As is discussed in Section 3.3, plasma in the plasma sheet is often not in thermal equilibrium and the particle distribution cannot be described by a Maxwellian distribution.

[6] We have used measurements from three of the five THEMIS spacecraft (TH-b, c, and d. Since TH-a, d, e are very close to each other in time and space, we used only TH-d) from March 23, 2007 to August 31, 2011. The THEMIS spacecraft move in low latitude orbits. During our selected period, TH-d covers regions inside r ∼12 R_E while TH-b and c cover regions inside r ∼30 R_E. Since October 2010 TH-b and c moved outward to circular orbits at r ∼40 to 70 R_E.

[7] For THEMIS, the ions and electrons are measured by an electrostatic analyzer (ESA, 0.006 − 20 keV/q for ions and 0.007 − 26 keV for electrons [*McFadden et al.*, 2008]) and a solid state telescope (SST, 35 keV − 6 MeV for ions and 30 keV − 6 MeV for electrons). Full distribution data are used. The data have time resolutions of ∼1.6 min during fast survey and ∼6.4 min during slow survey. For each measured energy spectrum, contamination to ESA and SST is removed. The penetrating radiation contamination is removed from the ESA data by subtracting the minimum count value within the ESA energy ranges (see Appendix of *Wang et al.* [2011] for details). However, there is not yet a method to satisfactorily remove the penetrating radiation contamination to SST. The sunlight contamination to the SST is removed (defined by a criteria that considers a data point being contaminated if its modified z-score calculated across azimuthal angle is greater than 3.5. The modified z-score is a normalized outlier detection test [*Iglewicz and Hoaglin*, 1993]. For a data point with value x_i, its modified z-score is $0.6745 \cdot (x_i - x_{median})/\text{median}(|x_i - x_{median}|)$. For ions, there is an energy gap (from ∼20 to 28 keV) between the highest ESA channel and the lowest SST channel. We interpolate the fluxes over this energy gap using the fluxes from the two nearby energy channels. That is, using the differential flux j_1 at E_1 (the highest ESA ion energy) and j_2 at E_2 (the lowest SST ion energy), we estimated j at E (the energy of the gap, $E = (E_1 + E_2)/2$) to be $j = 10^A$, where $A = \log_{10}(j_1)/2 + \log_{10}(j_2)/2$. The contribution to the total temperature from the ions within the gap can be from ∼1% to up to 20% of the temperature contributed by the rest of ions. The total plasma temperature is computed from the combined ESA and SST energy spectrum. In this study, we only included measurements when both Ti and Te are nearly isotropic, that is, $0.9 \le T_{i,\perp}/T_{i,\parallel}$ (and $T_{e,\perp}/T_{e,\parallel}$) ≤ 1.1. We excluded the data inside r = 6 R_E since in this region there can be large temperature uncertainty due to radiation contamination to SST during strong geomagnetic activities.

[8] We identified each THEMIS crossing of the bow shock and magnetopause and sorted each measurement into being within the magnetosheath and magnetosphere. Inside the magnetosphere, we included only data within the plasma sheet using a β criterion. The plasma sheet is centered at the equatorial plane. Central plasma sheet crossings are selected when plasma β (defined as $(P_{ion} + P_{electron})/(B^2/(2\ \mu_0))$ satisfies the criteria: $\beta \ge 1$, for $r \ge 15\ R_E$ and $\beta \ge 10^{0.14r-2.1}$ for $r < 15\ R_E$. The β criterion is r dependent since β in the equatorial plane decreases with decreasing r. In the plasma sheet, we only selected data with $|V_\perp| \le 100$ km/s. Finally we computed spatial distributions of temperature and temperature ratios by sorting the selected data into 2 $R_E \times 2\ R_E$ bins in the *X-Y* plane according to the *X* and *Y* of the THEMIS spacecraft in the magnetosheath and magnetosphere (aberrated GSM coordinates, with the aberration angle determined by one hour averaged solar wind velocity, is used).

[9] The solar wind ion and electron temperatures are computed from the Wind solar wind experiment (SWE) measurements (0.007 to 24.8 keV/q) [*Ogilvie et al.*, 1995]. To correlate the temperatures in the magnetosheath and plasma sheet with the solar wind speed and IMF, we used the OMNI data that has been time shifted to the bow shock nose. Both the Wind and OMNI data are obtained from the NASA CDAWeb.

3. Temperatures and Temperature Ratio

3.1. Overview

[10] Figure 1a shows an example of the ion and electron temperatures and their ratios in the magnetosheath and

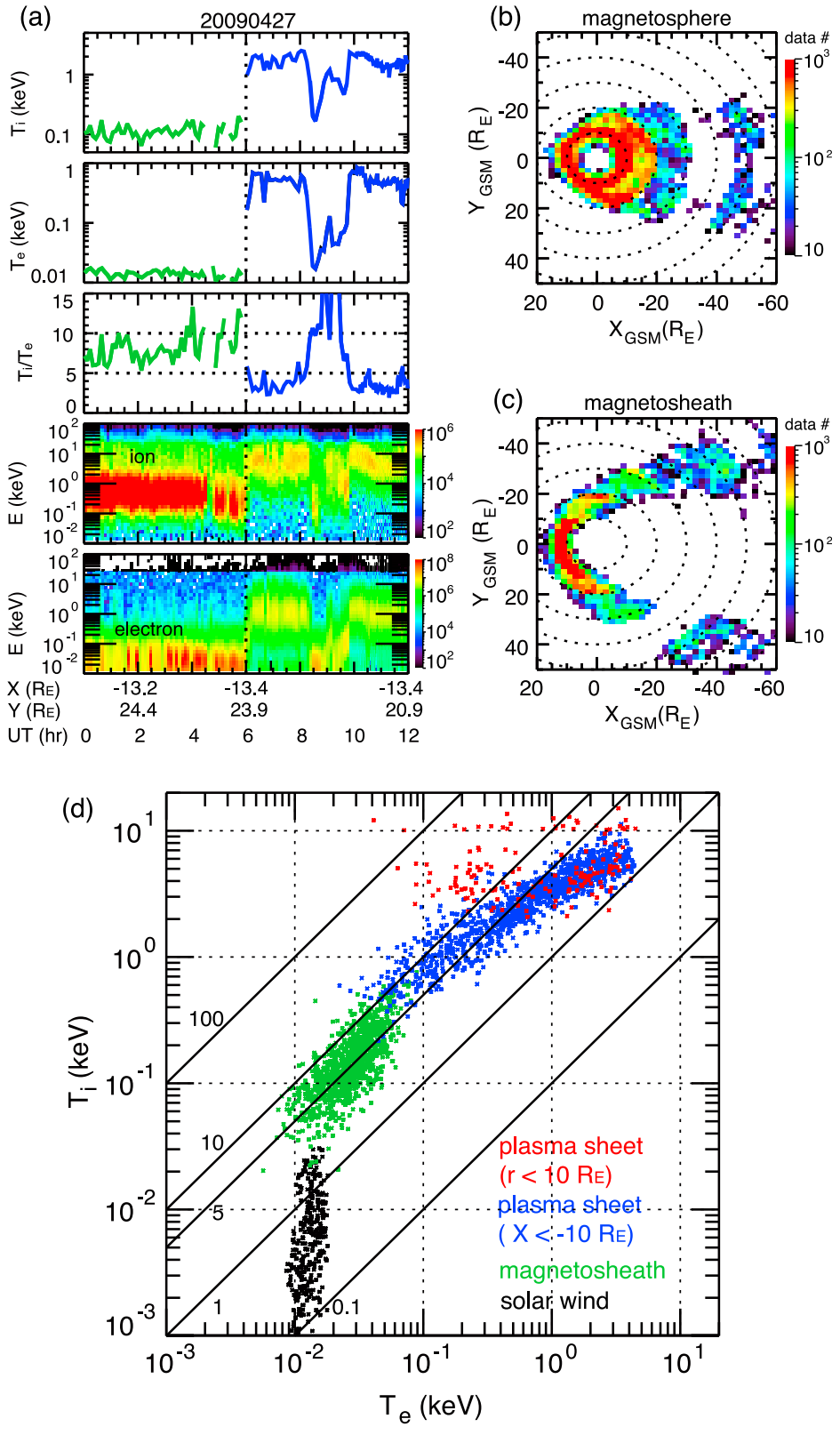
(a)
20090427
Ti (keV)
Te (keV)
Ti/Te
E (keV)
ion
electron
X (RE) -13.2 -13.4 -13.4
Y (RE) 24.4 23.9 20.9
UT (hr) 0 2 4 6 8 10 12
(b)
magnetosphere
data #
YGSM (RE)
XGSM(RE)
(c)
magnetosheath
(d)
Ti (keV)
Te (keV)
100
10
5
1
0.1
plasma sheet
(r < 10 RE)
plasma sheet
(X < -10 RE)
magnetosheath
solar wind

Figure 1

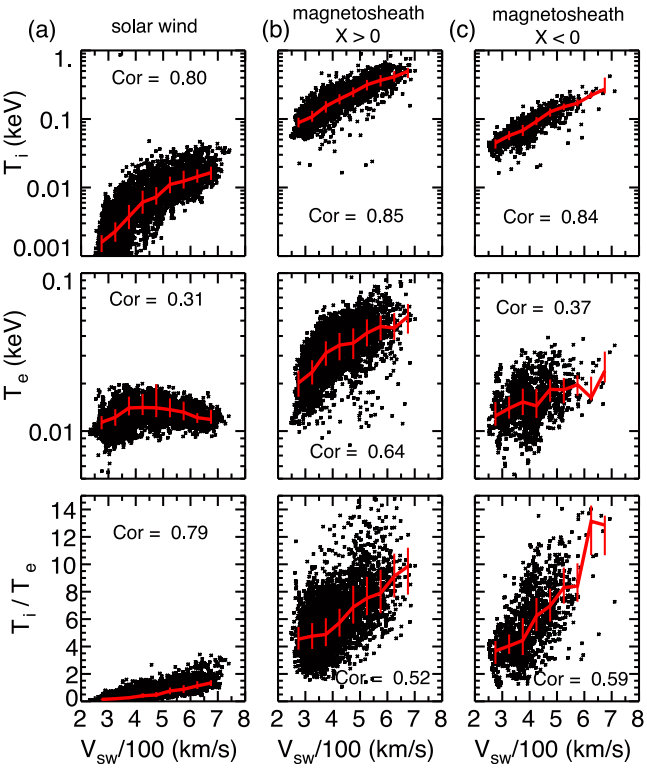

Figure 2. T_i, T_e, and T_i/T_e versus the solar wind speed in region of (a) the solar wind, (b) dayside magnetosheath, and (c) nightside magnetosheath. The red curves show median values with the red vertical lines indicate the ranges 25% and 75% percentiles. (Unless otherwise indicated, the curves in the figures of this paper for statistical results show median values while the vertical lines indicate the ranges of 25% and 75% percentiles.) The number in each plot indicates the linear correlation coefficient.

plasma sheet measured by THEMIS-b as the spacecraft crossed the duskside magnetopause. T_i, T_e, and T_i/T_e in the magnetosheath are seen to be distinguishably different from those in the plasma sheet. Within the plasma sheet, there are large variations in the temperature ratio, which are anti-correlated with the temperature variations. In this study, we investigate the variations of temperatures and temperature ratios statistically. The spatial distributions of the number of THEMIS measurements in the plasma sheet and magnetosheath selected for this study are shown in Figures 1b and 1c. Figure 1d gives an overview of how T_i is correlated with T_e in the solar wind, the magnetosheath, and the plasma sheet. It can be seen from Figure 1d that the ion temperature increases by 4 orders of magnitude and electron temperature by 3 orders of magnitude from the solar wind to the near-Earth magnetosphere. The temperature ranges for the regions of the solar wind, the magnetosheath, and the plasma sheet are well separated from each other, indicating that particles are energized as they go through the bow shock and magnetopause. Figure 1d also shows that T_i/T_e is not constant as temperature changes and varies significantly from a lowest of ~0.1 in the solar wind to a highest of ~100 in the near-Earth magnetosphere.

[11] As shown in Figure 1d, in the solar wind, T_i varies from ~0.001 to 0.03 keV while T_e remains within a much narrower range of ~0.01 to 0.02 keV. As a result, T_i/T_e increases from ~0.1 to 3 with increasing T_i. As discussed in Section 3.2.1, the variation is mainly controlled by the solar wind speed. In the magnetosheath, T_i increases with increasing T_e and T_i/T_e increases from ~2 to 10. The variation, as discussed in Section 3.2, depends on both location and solar wind speed. In the tail plasma sheet ($X < -10\ R_E$), T_i increases with increasing T_e but T_i/T_e decreases from above 10 to ~2. As discussed in Section 3.3, the ratio is controlled by mixture of cooler and warmer plasma sheet particles and the mixing shows strong dependences on spatial locations, as well as on the IMF condition and AE level. In the near-Earth magnetosphere ($r \le 10\ R_E$), T_i does not correlate with T_e and there is a much larger variation in T_e than in T_i. T_i/T_e ranges from ~1 to 100 and the ratio, as discussed in Section 3.5, is found to strongly depend on magnetic local time.

3.2. Temperature Ratio in the Magnetosheath

3.2.1. Dependence on the Solar Wind Speed

[12] Magnetosheath particles are solar wind particles energized by the bow shock. In the upstream solar wind, as shown in Figure 1a, T_i is often different from T_e. As shown in Figure 2a, in the solar wind T_i increases with increasing solar wind speed (V_{sw}) while T_e does not. As a result, T_i/T_e is higher when V_{sw} is larger. $T_i/T_e = 1$ occurs most frequently when V_{sw} is around 500 km/s. The above correlations of T_i and T_e with V_{sw} are consistent with previous studies [e.g., *Matthaeus et al.*, 2006; *Issautier et al.*, 2005].

[13] Comparing the temperature between the solar wind shown in Figure 2a and the magnetosheath in Figures 2b and 2c indicates that the bow shock energizes ions more than electrons, resulting in T_i/T_e in the magnetosheath being higher than that in the solar wind. The bow shock energization depends on V_{sw}. For electrons, the energization is much larger under higher V_{sw} with a factor of ~2 (5) when V_{sw} is 300 (600) km/s. For ions, the energization is almost 2 orders of magnitude when V_{sw} is 300 km/s but decreases to a factor of ~30 when V_{sw} is 600 km/s. Combing the two effects from the solar wind temperature and the bow shock energization and their dependences on V_{sw} leads to T_i in the magnetosheath increasing more with increasing V_{sw} than does T_e. As a result, the magnetosheath T_i/T_e becomes larger as V_{sw} increases. We have examined T_i/T_e with all solar wind parameters and found

Figure 1. (a) T_i, T_e, T_i/T_e, and energy spectrums of ion and electron energy fluxes (eV/(s-sr-cm^2-eV)) observed by THEMIS-b as it crossed the magnetopause (indicated by the dotted vertical lines) on 20090427. In the T_i, T_e, T_i/T_e curves, green indicates magnetosheath region while blue indicates plasma sheet region. Number of data selected for (b) the plasma sheet and (c) magnetosheath. (d) Scatter diagram of ion temperature (T_i) versus electron temperature (T_e) in the solar wind, magnetosheath, and plasma sheet. $T_i/T_e = 0.1$, 1, 5, 10, and 100 are indicated by the solid oblique lines. (Only every 40th point in the magnetosheath and the plasma sheet at $X < -10\ R_E$ and only every 200th point in the plasma sheet at $r < 10\ R_E$ is plotted.)

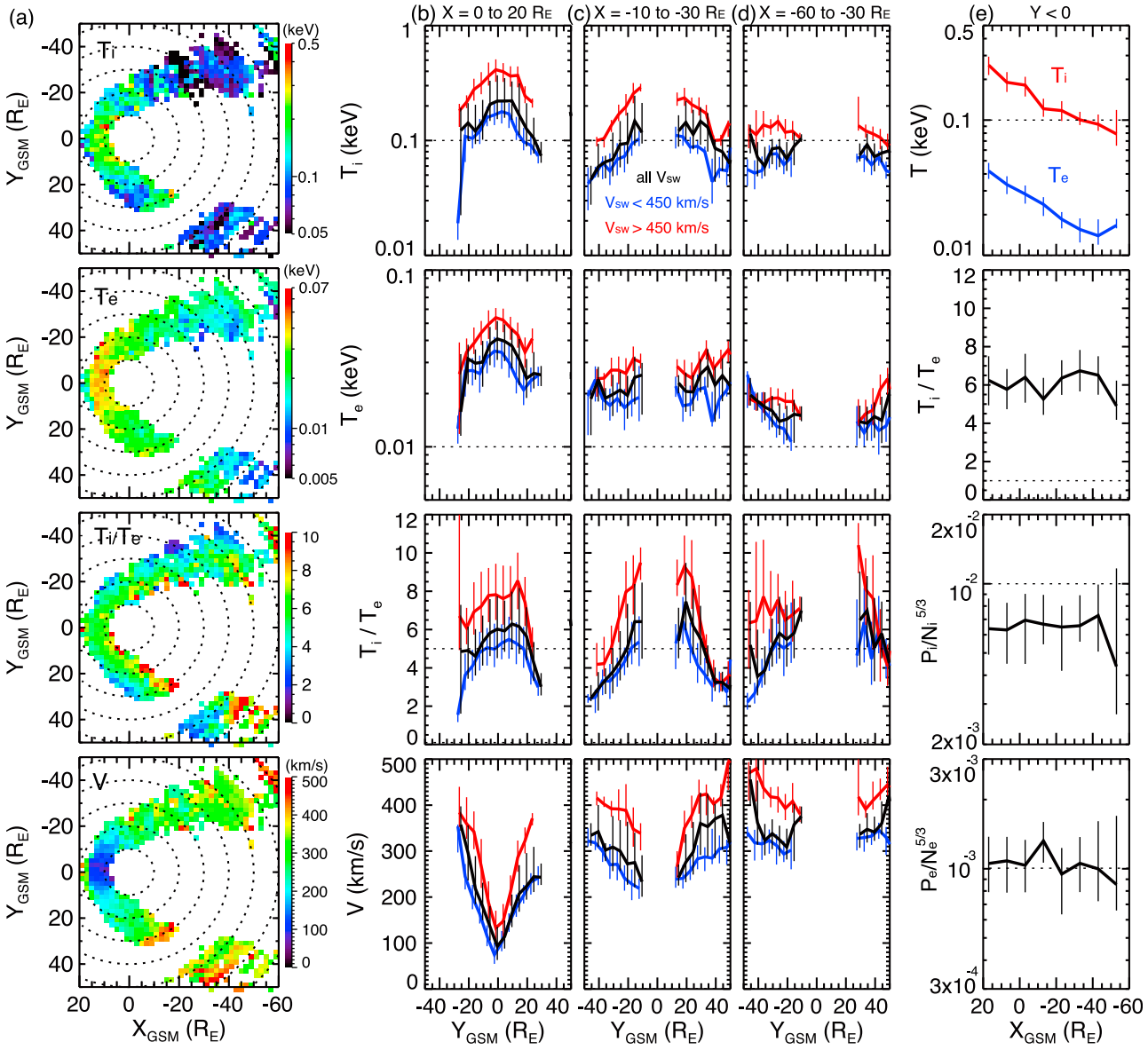

Figure 3. (a) From top to bottom, T_i, T_e, T_i/T_e, and flow speed (V) in the magnetosheath in the X-Y plane. The Y-profiles of T_i, T_e, T_i/T_e, and V at (b) X = 20 to 0 R_E, (c) X = −10 to −30 R_E, and (d) X = −30 to −60 R_E. The black curves show results for all upstream V_{sw}, the blue curves show results for $V_{sw} < 450$ km/s and the red curves for $V_{sw} > 450$ km/s. (e) The X-profiles (including the dawnside magnetosheath data at all *Y* within the same *X* range) of T_i, T_e, T_i/T_e, ion specific entropy $P_i/N_i^{5/3}$ (nPa-cm^5), and electron specific entropy $P_e/N_e^{5/3}$ (nPa-cm^5) along the dawnside magnetosheath.

that T_i/T_e is best correlated with V_{sw} (good correlations can also be found with the solar wind density and Mach number since these two parameters are well correlated with V_{sw}).

3.2.2. Spatial Distribution

[14] Figure 3a shows the spatial distributions of magnetosheath T_i, T_e, T_i/T_e, and flow speed in the X-Y plane with their Y profiles at different X ranges shown in Figures 3b to 3d. Since magnetosheath T_i, T_e, and T_i/T_e are correlated with V_{sw}, we also plot the Y profiles for different V_{sw} ranges to show that these spatial variations are real and not due to data selection biased by different V_{sw}. Both T_i and T_e are highest near the subsolar point where flow speed is the smallest because particles are heated as they are slowed down by the bow shock and as they approach the magnetopause. T_i and T_e decrease with increasing downtail distance from the subsolar point as flow speed increases back to almost the solar wind speed (the change can be also seen in Figures 3b–3d).

[15] At the same X, T_i shown in Figures 3b–3d is seen to decrease while the flow speed increases with increasing Y distance away from the magnetopause. On the other hand, for T_e, a decrease with increasing Y is only seen on the dayside and the decrease is less than that for ions. T_e on the nightside does not vary substantially along the Y-direction.

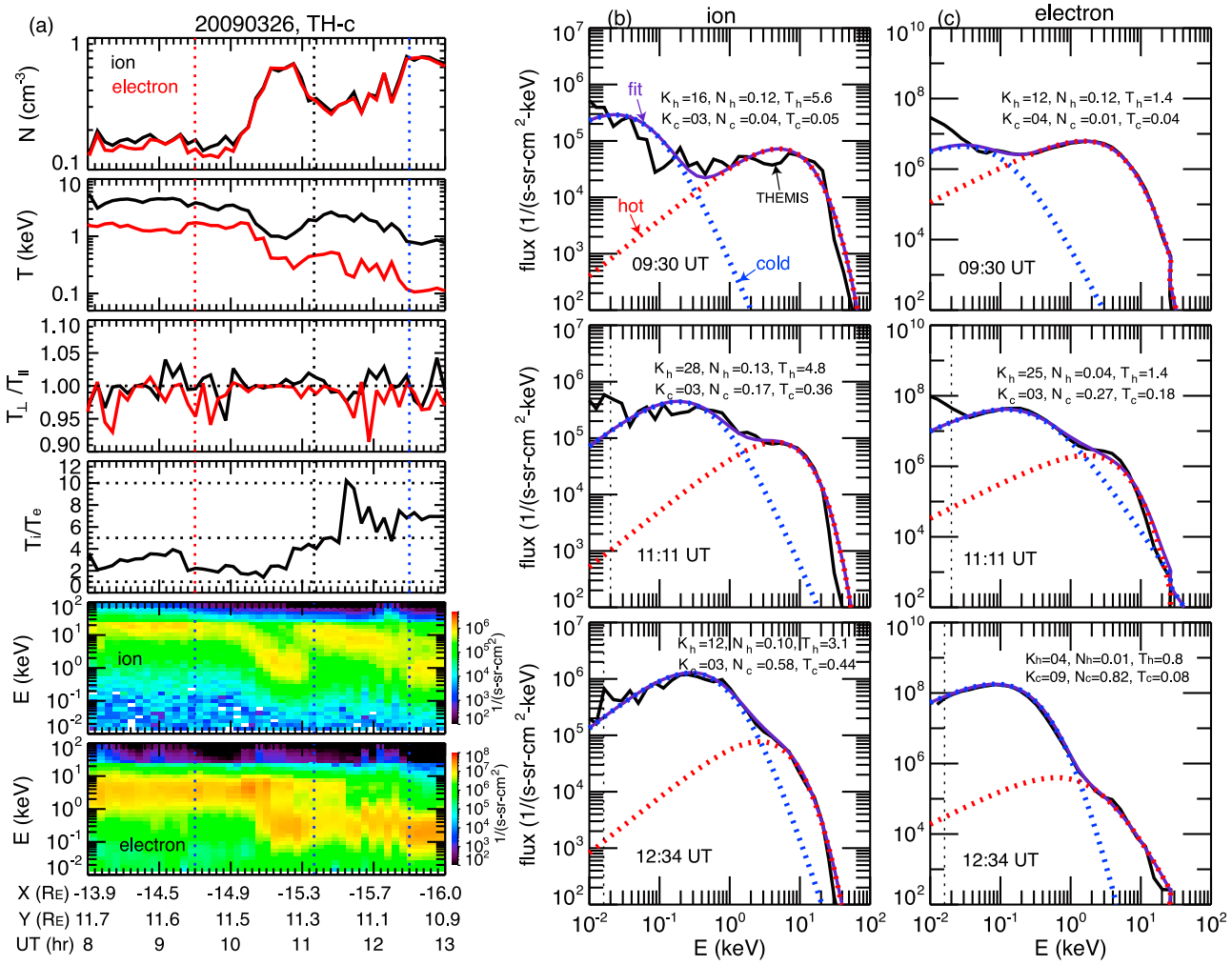

Figure 4. (a) From top to bottom, N, T, $T_\perp/T_\parallel$ (the black curves are for ion and the red curves for electrons), T_i/T_e, and energy spectrums of ion and electron energy fluxes observed by THEMIS-c on 20090326. Energy spectrum of (b) ion and (c) differential fluxes at three different times (09:30, 11:11 and 12:34 UT) indicated by the dashed vertical lines in Figure 4a. The black solid curves are observed fluxes and the purple solid curves are the fitted fluxes. The red (blue) dotted curves are the fitted hot (cold) component with their corresponding κ, N, and T listed on each plot.

As a result, T_i/T_e is the largest (~5 to 10) near the magnetopause and decreases quickly with increasing |Y|. In contrast to the strong T_i/T_e variation along the Y-direction, T_i/T_e does not change much with downtail distance. Figure 3e shows the X-profiles of the dawnside magnetosheath T_i/T_e and specific entropy for ions ($P_i/N_i^{5/3}$) and electrons ($P_e/N_e^{5/3}$) for data whose corresponding V_{sw} is between 400 and 500 km/s, where P is plasma pressure and N is number density (the duskside profiles are similar but are not shown since there is a data gap at r ~ 20 to 40 R_E). The almost X-independent T_i/T_e and specific entropy indicate that adiabatic cooling is responsible for the temperature decrease while keeping T_i/T_e constant. Note that the sudden drop of $P_i/N_i^{5/3}$ and T_i/T_e at $X = -55$ R_E is likely due to that the data coverage in Y beyond $X = -50$ R_E, as shown in Figure 3a, is too limited to give statistical values as good as those for $X > -50$ R_E. The variations of T_i and flow speed with the downtail distance qualitatively agree with the prediction of the Spreiter gasdynamic model [*Spreiter et al.*, 1966].

3.3. Temperature Ratio in the Tail Plasma Sheet Beyond X = −10 R_E

3.3.1. Dependence of the Ratio on Ion Temperature

[16] Figure 1d shows that in the tail plasma sheet beyond X = −10 R_E, T_i/T_e decreases with increasing T_i or T_e. Figure 4a shows the plasma sheet observed by THEMIS-c on 26 March 2009 at (X ~ −15, Y ~ 11 R_E) and it can be seen that T_i/T_e increased as the plasma became colder. While both T_i and T_e decreased, the increase of T_i/T_e is mainly due to T_e decreasing more significantly than T_i. As shown in the energy spectra in Figures 4a–4c, the plasma sheet particle population is often a mixture of one colder and one hotter population, indicating the particles are not in thermal equilibrium. The total temperature of the whole population is thus determined by the thermal temperatures of these two populations and their relative abundance. The mixture can be accounted for by a two-component Maxwellian or kappa distribution [*Wing et al.*, 2005; *Wang et al.*, 2007]. To

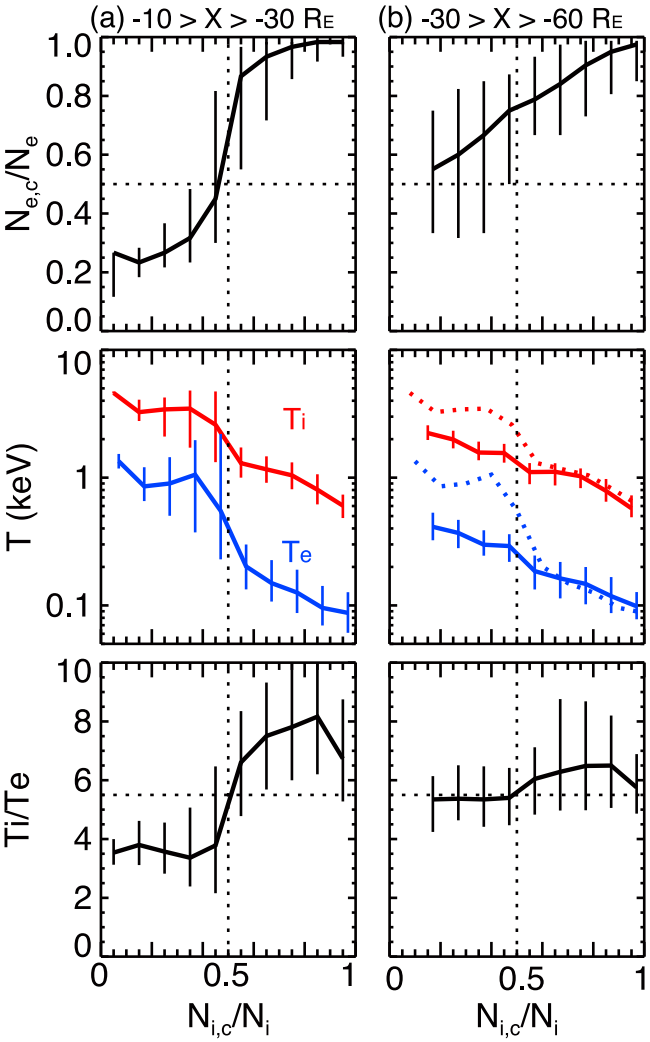

Figure 5. $N_{e,c}/N_e$, T_i (the red curves), T_e (the blue curves), and T_i/T_e versus $N_{i,c}/N_i$ in region of (a) $-10 > X > -30$ R_E and (b) $-30 > X > -60$ R_E. The dashed T_i and T_e curves in Figure 5a are superimposed as the dashed curves in Figure 5b.

understand how the mixture of colder and hotter populations affects T_i/T_e, we fitted each observed ion and electron energy spectrum with a two-component kappa distribution,

$$f = N_c\left(\frac{m}{2\pi\kappa_c E_{0,c}}\right)^{3/2}\frac{\Gamma(\kappa_c+1)}{\Gamma(\kappa_c-1/2)}\left[1+\frac{E}{\kappa_c E_{0,c}}\right]^{-\kappa_c-1}$$

$$+N_h\left(\frac{m}{2\pi\kappa_h E_{0,h}}\right)^{3/2}\frac{\Gamma(\kappa_h+1)}{\Gamma(\kappa_h-1/2)}\left[1+\frac{E}{\kappa_h E_{0,h}}\right]^{-\kappa_h-1}$$

where f is phase space density, N is density, m is particle mass, and κ and E_0 are parameters of the kappa distribution (subscript c is for cold population and h is for hot populations, $E_0 = k_B T_0(1–3/2\kappa)$ is the energy of the peak particle flux). N, κ, and E_0 are free parameters in the fitting. Note that when N_h is much smaller than N_c or vice versa, then a two-component distribution becomes essentially a one-component distribution. The fitted total density is $(N_h + N_c)$ and total temperature is $(N_h T_{0,h} + N_c T_{0,c})/(N_h + N_c)$. We only used data points for which the fitted total density and temperature are within 10% error of those calculated from the observed data. The fitted distributions and the values of the parameters are shown along with the observations in Figures 4b and 4c. Regardless the IMF Bz direction, most of the magnetosphere data selected for this study have T_h substantially larger than T_c, that is, the hot and cold populations are well separated. In this paper, we refer plasma sheet plasma to be "cool" ("warm") when $N_{i,c}/N_i \geq 0.5$ ($\leq$0.5), where N_i is ion density.

[17] Figure 5 shows statistical results of how $N_{e,c}/N_e$, T_i, T_e, and T_i/T_e change as the cold component of ions ($N_{i,c}/N_i$) becomes more dominant. Figure 5b shows that in the distant-tail plasma sheet ($X < -30$ R_E), $N_{e,c}/N_e$ increases with increasing $N_{i,c}/N_i$, thus T_e decreases together with T_i. T_i/T_e increases only slightly from ~5–6 when ions are warm to ~6–7 when ions are cool. Interestingly, despite the electron mixture changing linearly with the ion mixture, when ions become dominated by the hot component (that is, $N_{i,c}/N_i < 0.5$), the electrons remain dominated by the cold component ($N_{e,c}/N_e > 0.5$). However, as shown in Figure 5a, the correlation between the electron mixture and the ion mixture becomes nonlinear in the near-Earth tail plasma sheet ($X > -30$ R_E). When ions are warm, $N_{e,c}/N_e$ is ~0.3 and increases very slightly with increasing $N_{i,c}/N_i$. There is a sharp jump of $N_{e,c}/N_e$ from below 0.4 to above 0.8 as ions switches from being warm to cool. $N_{e,c}/N_e$ then stays high (~0.9) as ions become cooler. As a result, in the near-Earth tail plasma sheet, T_i/T_e in warm plasma (~4) is distinguishably different from that in cool plasma (~7). Likely causes for the differences seen in warm plasma between the near-Earth and distant tail plasma sheet is discussed in Section 3.3.2 and 3.3.3.

3.3.2. Spatial Distribution

[18] Figure 6 shows the equatorial distributions of the plasma sheet T_i, T_e, and T_i/T_e. Their cross-tail profiles are shown in Figures 6b and 6c, together with the profiles for the cool and warm plasma and the occurrence rate of cool plasma. In the distant tail shown in Figure 6c, the occurrence rate for cool plasma is high except near midnight. T_i and T_e for both cool and warm plasma vary only slightly across the tail. Except near the duskside flank, T_i/T_e is ~4 to 6 and it has no significant variation in Y and has only slight difference between cool and warm plasma. Quite different spatial distributions are seen in Figure 6b for the near-Earth tail. For both cool and warm plasma, T_i and T_e are relatively lower near the two flanks than at midnight. T_i/T_e of warm plasma varies little across the tail, while that of cool plasma increases by a factor of 2 from midnight to the dusk flank. T_i/T_e of warm plasma (~3 to 5) is well separated from that of cool plasma (~5 to 10) in the near-Earth tail and is clearly lower than that of warm plasma in the distant tail. The occurrence rate of cold plasma is high near the two flanks and decreases to very low at midnight, which is due to colder magnetosheath particles entering from the flanks and then moving slowly toward midnight [e.g., *Wang et al.*, 2010]. Therefore, higher T_i/T_e is more often observed at larger |Y|. There is a dawn-dusk asymmetry in the T_i/T_e of cool plasma due to the relatively lower T_i (higher T_e) near the dawn flank than the dusk flank. The temperature differences are mainly

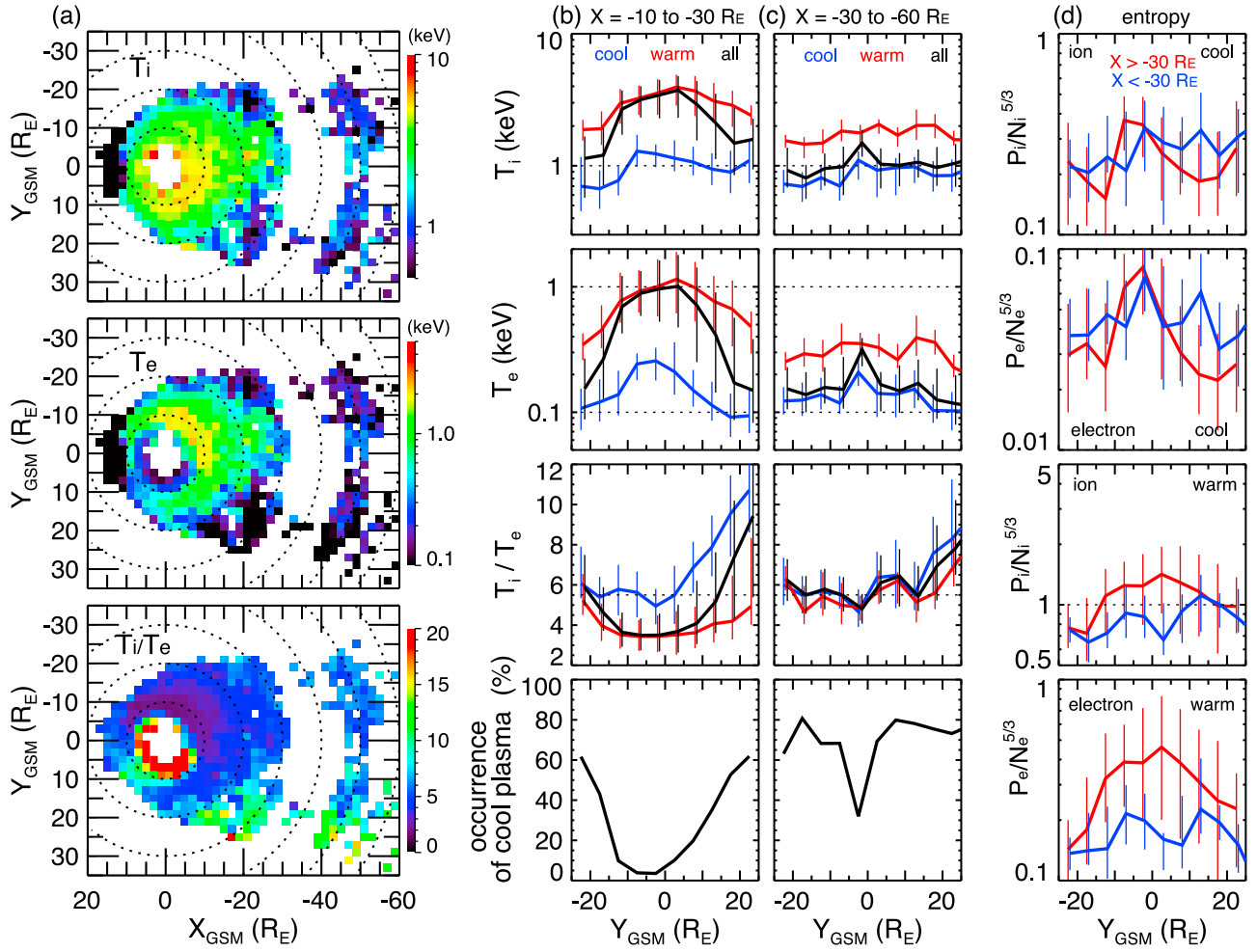

Figure 6. (a) T_i, T_e, T_i/T_e in the plasma sheet in the X-Y plane. The Y-profiles of T_i, T_e, T_i/T_e, and the occurrence rate of cool plasma in region of (b) $-10 > X > -30$ R_E and (c) $-30 > X > -60$ R_E for all plasma (the black curves), warm plasma (the red curves), and cool plasma (the blue curves). (d) Comparisons of the Y-profiles of ion specific entropy $P_i/N_i^{5/3}$ (nPa-cm^5) and electron specific entropy $P_e/N_e^{5/3}$ (nPa-cm^5) between the two X regions (the red curves for $X > -30$ R_E and the blue curves for $X < -30$ R_E) when plasma is cool (the top two plots) and when plasma is warm (the bottom two plots).

a result of dawn-dusk differences in $N_{i,c}/N_i$ ($\sim$0.9 near the dawn flank and $\sim$0.8 near the dusk flank) and $N_{e,c}/N_e$ (<0.95 near the dawn flank and >0.95 near the dusk flank) with $T_{i,h}$, $T_{i,c}$, $T_{e,h}$ and $T_{e,c}$ being relatively dawn-dusk symmetric. Note that $T_{i,c}$ in this study is found to become relatively higher near the dawn than the dusk flank under northward IMF, consistent with the dawn-dusk asymmetry reported by previous studies using Geotail [*Hasegawa et al.*, 2004] and DMSP [*Wing et al.*, 2005] for the northward IMF plasma sheet.

[19] Figure 6d compares the specific entropy of warm and cool plasma between the distant tail and near-Earth tail. For cool plasma, entropy changes are very small. For warm plasma, the particles near midnight clearly gain entropy as they move from the distant to near-Earth tail while those near the flanks do not. This suggests that as warm and cool particles move earthward and are adiabatically energized, an additional non-adiabatic process preferentially heats the warm particles in the near-Earth midnight region. Such non-adiabatic heating can be substorm or flow burst related and is possibly through wave-particle interactions or reconnection. In addition, the increase in entropy appears larger for electrons than ions, suggesting that the non-adiabatic process energizes electrons more than ions, leading to lower T_i/T_e of warm plasma near midnight compared with that in the distant tail.

3.3.3. Dependence on the Solar Wind, IMF, and AE

[20] Since T_i/T_e in the tail plasma sheet depends strongly on plasma being cool or warm, T_i/T_e should also depend on the solar wind or geomantic activity conditions that are closely correlated with the number of cold or hot particles in the plasma sheet. Since plasma sheet becomes colder under longer or stronger northward IMF [e.g., *Terasawa et al.*, 1997; *Wing et al.*, 2005; *Wang et al.*, 2010], T_i/T_e is higher under northward than southward IMF, as shown in Figure 7a. After onset of a substorm, a decrease in colder particles and an increase in hotter particles is often seen in the near-Earth tail at near midnight MLTs [e.g., *Lyons et al.*, 2003], thus the near-Earth plasma sheet is found to be warmer during higher AE levels [e.g., *Wang et al.*, 2009].

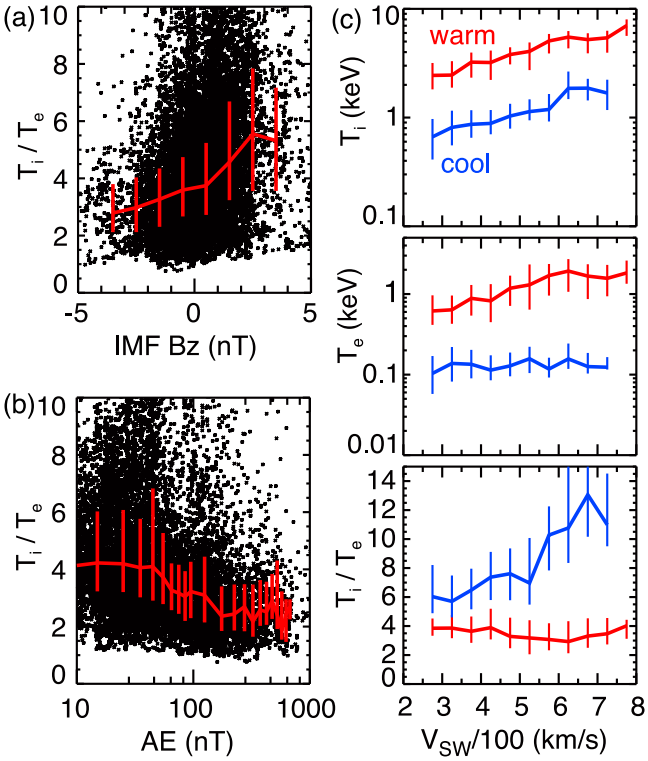

Figure 7. T_i/T_e versus (a) 2 h average IMF Bz and (b) 1 h average AE. (c) T_i, T_e, T_i/T_e versus V_{sw} for cool plasma (the blue curves) and warm plasma (the red curves).

Therefore, lower T_i/T_e is more often seen when AE is higher as shown in Figure 7b, and is likely caused by substorm related non-adiabatic heating.

[21] Figure 7c shows that in the tail plasma sheet both T_i and T_e increase with increasing V_{sw}. When plasma is warm, T_i/T_e is independent of V_{sw}. However, when plasma is cool, T_i/T_e increases as V_{sw} gets higher. This is similar to the dependence of the magnetosheath T_i/T_e on V_{sw} as shown in Figure 2c, suggesting a close correlation between the cool plasma sheet particles and magnetosheath particles. This is further discussed below.

3.4. Changes of Temperature Ratio Across the Magnetopause

[22] Figures 8a and 8b show how T_i/T_e changes across the duskside magnetopause during two different crossings by THEMIS-b. In both crossings, T_i/T_e is ~10 in the magnetosheath just outside the magnetopause. (Note that the very high T_i/T_e ~15 spikes seen outside the magnetopause indicated by the black curves are due to the existence of hot ions leaking out from the magnetosphere, and this hot ion plasma is distinguishably different from magnetosheath plasma in temperature and drift speed). Inside the magnetosphere, T_i/T_e is roughly the same as that in the magnetosheath when the plasma sheet plasma is cool, as shown in the November 18 2010 crossing. However, when the plasma sheet plasma is warm, as seen in the April 27 2009 crossing, T_i/T_e drops sharply to ~3. The low energy particles seen in the cool plasma sheet next to the magnetopause are likely magnetosheath particles that just entered the magnetosphere and

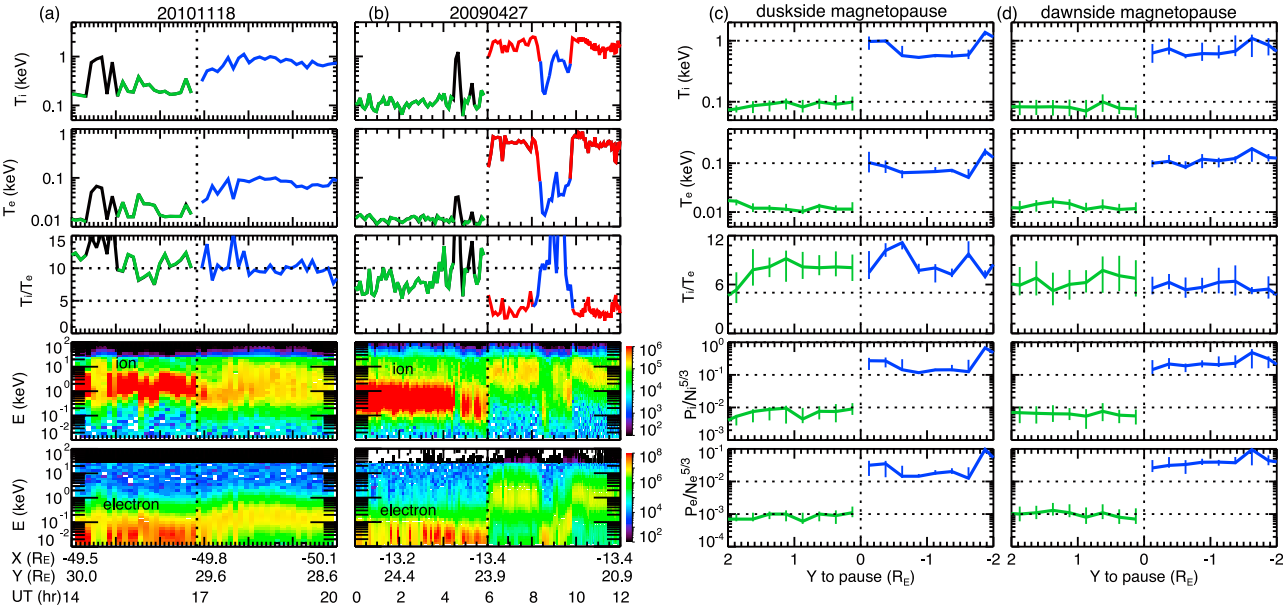

Figure 8. T_i, T_e, T_i/T_e, and energy spectrums of ion and electron energy fluxes (eV/(s-sr-cm^2-eV)) observed by THEMIS-b as it crossed the magnetopause (indicated by the dotted vertical lines) on (a) 20090423 and (b) 20090427. The green curves indicate magnetosheath plasma while the black curves indicate the hot plasma leaking out from the magnetosphere. The cool (warm) plasma sheet plasma are indicated by the blue (red) curves. T_i, T_e, T_i/T_e, ion specific entropy $P_i/N_i^{5/3}$ (nPa-cm^5) and electron specific entropy $P_e/N_e^{5/3}$ (nPa-cm^5) versus the Y-distance to the magnetopause (positive Y for the magnetosheath and negative Y for the plasma sheet) at (c) the duskside magnetopause and (d) the dawnside magnetopause.

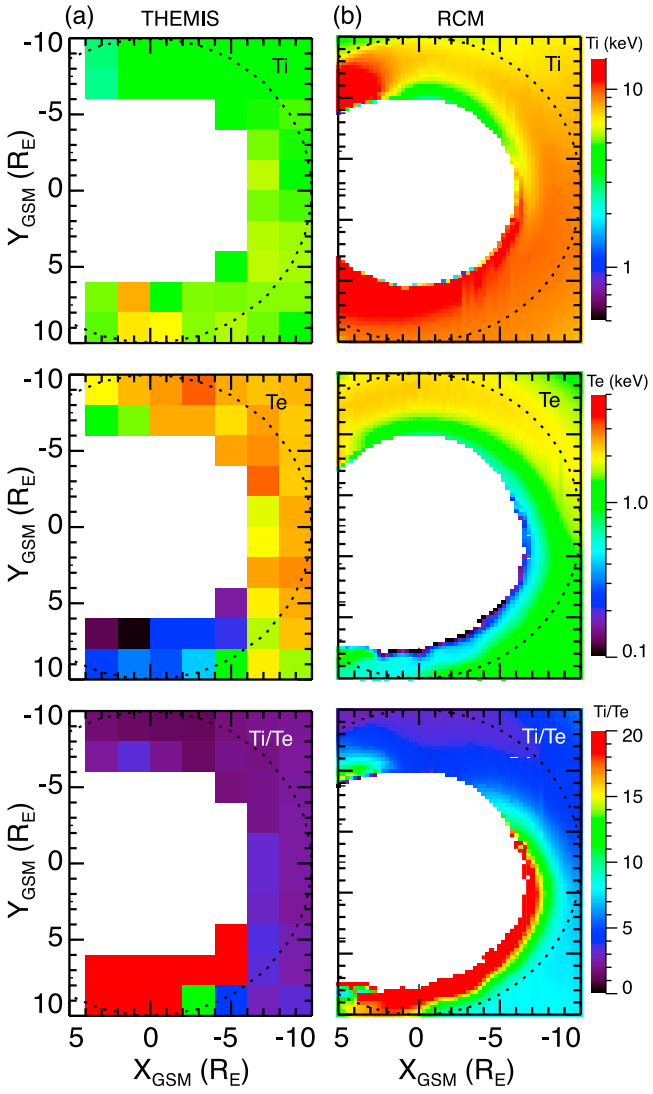

Figure 9. T_i, T_e, T_i/T_e, in the near-Earth magnetosphere in the X-Y plane from (a) THEMIS and (b) the RCM.

were energized at the magnetopause. Possible entry mechanisms include the Kelvin-Helmholtz instability [e.g., *Fujimoto and Terasawa*, 1994; *Otto and Nykyri*, 2003], diffusion by kinetic Alfven waves [e.g., *Johnson and Cheng*, 1997], and high latitude reconnection [e.g., *Song and Russell*, 1992; *Li et al.*, 2008].

[23] Figures 8c and 8d show statistically the changes of T_i/T_e from the magnetosheath to cool plasma sheet at the duskside (21 crossings) and dawnside magnetopause (34 crossings) beyond X = −40 R_E, respectively. For both ions and electrons, temperature increases by a factor of ∼6 to 10 and specific entropy increases by a factor of ∼20 from the magnetosheath to the plasma sheet while T_i/T_e remains roughly similar, indicating non-adiabatic heating that increases both the ion and electron temperature by almost the same proportion. There is also no clear difference in these increases between the dawnside and duskside magnetopause. These results can be used to evaluate the importance of the above entry mechanisms in future studies.

3.5. In the Near-Earth Magnetosphere

[24] Figure 1d shows that T_i/T_e in the near-Earth magnetosphere (r < 10 R_E) varies significantly from ∼1 to almost 100. As can be seen in Figure 6a the distributions for all IMF conditions and Figure 9a for southward IMF, higher T_i/T_e (>15) is seen at the dusk MLTs and lower T_i/T_e (<3) at the dawn MLTs. The asymmetry is due to strong dawn-dusk asymmetries in both T_i and T_e with their asymmetries being opposite to each other with higher T_i (T_e) at the dusk (dawn) MLTs. The electron asymmetry is stronger than the ion asymmetry. That the asymmetries become stronger closer to the Earth and electron and ion have opposite asymmetries suggests that they are likely a result of energy- and species-dependent magnetic drift.

[25] To examine the effect of magnetic drift on the MLT distributions of T_i/T_e, we compared the observations with the simulation results of the Rice Convection Model (RCM) from our previous study [*Gkioulidou et al.*, 2011]. The RCM computes electric and magnetic drift transport of ions and electrons of different energies and allows for mixing of particles drifting from different locations. In the RCM simulation run, the electric and magnetic drift of ions and electrons are simulated under self-consistent electric and magnetic field and the particle sources at the nightside outer boundary (the outer boundary is defined by a 15 R_E circle with its center at $X = -5$ R_E and $Y = 0$, so it is at r ∼15 R_E at dawn and dusk and at 20 R_E at midnight) are based on statistical results of Geotail observations for southward IMF (see *Gkioulidou et al.* [2011] for detailed descriptions of the simulation setup). In this RCM run, no initial particle distribution is specified to ensure that the simulated plasma sheet is formed by particles drifting from the outer boundary. Figure 9b shows the simulation results after 6 simulation hours. All the particles have occupied the nightside the plasma sheet, but the colder and slower particles have yet fully occupied the dayside, resulting in the very high T_i in the early morning sector. As can be seen from the comparison between the THEMIS and simulation results on the nightside shown in Figures 9a and 9b, there are quantitative differences between the observations and simulations with the RCM T_i being slightly higher and the RCM T_e lower than the observed temperatures. The differences are mainly contributed by the RCM boundary particle distributions used in this run (Geotail based) not exactly matching the THEMIS distributions at the RCM boundary locations. Nevertheless, the dawn-dusk asymmetries of T_i, T_e, and T_i/T_e on the nightside can be clearly seen in the RCM distributions and are qualitatively consistent with the THMEIS results. Analysis of the particle transport paths in the RCM shows that while particles electric drift earthward and are adiabatically energized, it is magnetic drift that diverts hotter ions further toward dusk and hotter electrons further toward dawn, creating the strong T_i/T_e asymmetry seen in the near-Earth magnetosphere.

4. Summary

[26] In this study, we have used 4 years of THEMIS data to determine the spatial distributions of T_i, T_e, and T_i/T_e in the magnetosheath and plasma sheet. T_i and T_e increase by at least an order of magnitude as particles move from the solar

wind to the magnetosheath and from the magnetosheath to magnetosphere. T_i/T_e is not a constant. It varies from ~0.1 to 2 in the solar wind, from ~4 to 12 in the magnetosheath, from ~2 to 12 in the tail plasma sheet, and from 1 to 100 in the near-Earth magnetosphere.

[27] T_i/T_e in the magnetosheath is found to be best correlated with V_{sw} among all solar wind and IMF parameters, with higher T_i/T_e during larger V_{sw}. Under the same V_{sw}, T_i/T_e decreases quickly away from the magnetopause along the same X. While T_i and T_e decrease significantly with increasing downtail distance from the subsolar point, T_i/T_e remains similar, and so does the ion and electron specific entropy, indicating adiabatic cooling of both ions and electrons as they move downstream.

[28] In the tail plasma sheet, T_i/T_e is well correlated with ion temperature, with higher T_i/T_e when ion temperature is lower. Ions in the plasma sheet are often a mixture of one colder and one hotter population, not just one single population like it is in the magnetosheath, so that temperature is determined by relative dominance of the colder or the hotter population. In the near-Earth tail, T_i/T_e is $<\sim 4$ when the hotter ions dominates but switches sharply to $>\sim 6$ when colder ions become dominant. Therefore, the plasma sheet T_i/T_e is also found to be well correlated with conditions that preferentially create more colder or hotter ions in the plasma sheet. Colder ions are more abundant, thus T_i/T_e is higher closer to the flanks and during northward IMF. A very low T_i/T_e (<2) is more often seen in the near-Earth tail around midnight when AE is high, which could be a result of an increase of hotter particles and a decrease of colder particles that has been seen after substorm onset. As ions and electrons move earthward from the distant tail and are adiabatically energized, the processes related to substorm or flow bursts may also cause an additional non-adiabatic heating that energizes electrons more than ions, resulting in a lower T_i/T_e.

[29] Many processes have been proposed for the magnetosheath particles entering into the magnetosphere to explain the abundance of cold plasma sheet particles near the flanks. Temperature of both ions and electrons are found to increase by a factor of ~6 to 10 and specific entropy to increase by a factor of ~20 across the magnetopause from the magnetosheath to the cool plasma sheet, while T_i/T_e and its dependence on the solar wind speed in either sides of the magnetopause are very similar. These indicate that non-adiabatic heating associated with the entry mechanism increases both T_i and T_e by almost the same proportion.

[30] A very strong T_i/T_e dawn-dusk asymmetry is seen in the near-Earth magnetosphere with very high T_i/T_e (~15 to 100) near dusk and very low T_i/T_e (~1) near dawn, which is due to strong but opposite dawn-dusk asymmetries in T_i and T_e with higher T_i (T_e) near dusk (dawn). These asymmetries are qualitatively consistent with the simulation results of the RCM, which shows that the asymmetries are caused by the energy-dependent magnetic drift bringing hotter ions (electrons) further toward dusk (dawn).

[31] **Acknowledgments.** The work by C.-P. Wang, M. Gkioulidou, and L. R. Lyons has been supported by NASA Grant NNX11AJ12G, NNX09AQ41H, and NNX08A135G, and NSF Grant ATM-0819864 and ATM-1003595. We acknowledge NASA contract NAS5–02099 for THEMIS, and C. W. Carlson and J. P. McFadden for the use of ESA data, D. Larson and R. P. Lin for use of the SST data. We thank J. H. King, N. Papatashvilli at AdnetSystems, NASA GSFC and CDAWeb for providing the OMNI data. We thank K. Ogilvie at NASA GSFC and CDAWeb for providing the WIND/SWE data. AE index was provided by World Data Center for Geomagnetism, Kyoto. We thank the support of ISSI International Teams Program: Plasma Entry and Transport in the Plasma Sheet.

[32] Masaki Fujimoto thanks the reviewers for their assistance in evaluating this paper.

References

Artemyev, A. V., W. Baumjohann, A. A. Petrukovich, R. Nakamura, I. Dandouras, and A. Fazakerley (2011), Proton/electron temperature ratio in the magnetotail, *Ann. Geophys.*, *29*(12), 2253–2257, doi:10.5194/angeo-29-2253-2011.

Baumjohann, W. (1993), The near-Earth plasma sheet: An AMPTE/IRM perspective, *Space Sci. Rev.*, *64*(1–2), 141–163, doi:10.1007/BF00819660.

Baumjohann, W., and R. A. Treumann (1996), *Basic Space Plasma Physics*, Imp. Coll. Press, London.

Baumjohann, W., G. Paschmann, and C. A. Cattell (1989), Average plasma properties in the central plasma sheet, *J. Geophys. Res.*, *94*(A6), 6597–6606, doi:10.1029/JA094iA06p06597.

Fujimoto, M., and T. Terasawa (1994), Anomalous ion mixing within an MHD scale Kelvin-Helmholtz vortex, *J. Geophys. Res.*, *99*(A5), 8601–8613, doi:10.1029/93JA02722.

Gkioulidou, M., C.-P. Wang, and L. R. Lyons (2011), Effect of self-consistent magnetic field on plasma sheet penetration to the inner magnetosphere: Rice convection model simulations combined with modified Dungey force-balanced magnetic field solver, *J. Geophys. Res.*, *116*, A12213, doi:10.1029/2011JA016810.

Hasegawa, H., M. Fujimoto, Y. Saito, and T. Mukai (2004), Dense and stagnant ions in the low-latitude boundary region under northward interplanetary magnetic field, *Geophys. Res. Lett.*, *31*, L06802, doi:10.1029/2003GL019120.

Iglewicz, B., and D. Hoaglin (1993), *How to Detect and Handle Outliers*, vol. 16, *The ASQC Basic References in Quality Control: Statistical Techniques*, edited by E. F. Mykytka, 87 pp., ASQC Quality, Milwaukee, Wis.

Issautier, K., C. Perche, S. Hoang, C. Lacombe, M. Maksimovic, J.-L. Bougeret, and C. Salem (2005), Solar wind electron density and temperature over solar cycle 23: Thermal noise measurements on Wind, *Adv. Space Res.*, *35*, 2141–2146, doi:10.1016/j.asr.2005.04.085.

Johnson, J. R., and C. Z. Cheng (1997), Kinetic Alfvén waves and plasma transport at the magnetopause, *Geophys. Res. Lett.*, *24*(11), 1423–1426, doi:10.1029/97GL01333.

Kaufmann, R. L., W. R. Paterson, and L. A. Frank (2005), Relationships between the ion flow speed, magnetic flux transport rate, and other plasma sheet parameters, *J. Geophys. Res.*, *110*, A09216, doi:10.1029/2005JA011068.

Lavraud, B., et al. (2009), Tracing solar wind plasma entry into the magnetosphere using ion-to-electron temperature ratio, *Geophys. Res. Lett.*, *36*, L18109, doi:10.1029/2009GL039442.

Li, W., J. Raeder, M. F. Thomsen, and B. Lavraud (2008), Solar wind plasma entry into the magnetosphere under northward IMF conditions, *J. Geophys. Res.*, *113*, A04204, doi:10.1029/2007JA012604.

Lyons, L. R., C.-P. Wang, T. Nagai, T. Mukai, Y. Saito, and J. C. Samson (2003), Substorm inner plasma sheet particle reduction, *J. Geophys. Res.*, *108*(A12), 1426, doi:10.1029/2003JA010177.

Matthaeus, W. H., H. A. Elliott, and D. J. McComas (2006), Correlation of speed and temperature in the solar wind, *J. Geophys. Res.*, *111*, A10103, doi:10.1029/2006JA011636.

McFadden, J. P., C. W. Carlson, D. Larson, J. Bonnell, F. Mozer, V. Angelopoulos, K.-H. Glassmeier, and U. Auster (2008), THEMIS ESA first science results and performance issues, *Space Sci. Rev.*, *141*, 477–508, doi:10.1007/s11214-008-9433-1.

Ogilvie, K. W., D. J. Chornay, R. J. Fritzenreiter, F. Hunsaker, J. Keller, J. Lobell, G. Miller, J. D. Scudder, E. C. Sittler, and R. B. Torbert (1995), SWE, a comprehensive plasma instrument for the WIND spacecraft, *Space Sci. Rev.*, *71*, 55–77, doi:10.1007/BF00751326.

Otto, A., and K. Nykyri (2003), Kelvin-Helmholtz instability and magnetic reconnection: Mass transport at the LLBL, in *Earth's Low-Latitude Boundary Layer*, *Geophys. Monogr. Ser.*, vol. 133, edited by P. T. Newell and T. Onsager, pp. 53–62, AGU, Washington, D. C., doi:10.1029/133GM05.

Paschmann, G., W. Baumjohann, N. Sckopke, T.-D. Phan, and H. Lühr (1993), Structure of the dayside magnetopause for low magnetic shear, *J. Geophys. Res.*, *98*(A8), 13,409–13,422, doi:10.1029/93JA00646.

Paterson, W. R., and L. A. Frank (1994), Survey of plasma parameters in Earth's distant magnetotail with the Geotail spacecraft, *Geophys. Res. Lett.*, *21*(25), 2971–2974, doi:10.1029/94GL02105.

Phan, T. D., G. Paschmann, W. Baumjohann, N. Sckopke, and H. Lühr (1994), The magnetosheath region adjacent to the dayside magnetopause:

AMPTE/IRM observations, *J. Geophys. Res.*, *99*(A1), 121–141, doi:10.1029/93JA02444.

Slavin, J. A., E. J. Smith, D. G. Sibeck, D. N. Baker, R. D. Zwickl, and S.-I. Akasofu (1985), An ISEE 3 study of average and substorm conditions in the distant magnetotail, *J. Geophys. Res.*, *90*(A11), 10,875–10,895, doi:10.1029/JA090iA11p10875.

Song, P., and C. T. Russell (1992), Model of the formation of the low-latitude boundary layer for strongly northward interplanetary magnetic field, *J. Geophys. Res.*, *97*(A2), 1411–1420, doi:10.1029/91JA02377.

Spreiter, J. R., A. L. Summers, and A. Y. Alksne (1966), Hydromagnetic flow around the magnetosphere, *Planet. Space Sci.*, *14*, 223–250, doi:10.1016/0032-0633(66)90124-3.

Terasawa, T., et al. (1997), Solar wind control of density and temperature in the near-Earth plasma sheet: WIND/GEOTAIL collaboration, *Geophys. Res. Lett.*, *24*, 935–938, doi:10.1029/96GL04018.

Wang, C.-P., L. R. Lyons, T. Nagai, J. M. Weygand, and R. W. McEntire (2007), Sources, transport, and distributions of plasma sheet ions and electrons and dependences on interplanetary parameters under northward interplanetary magnetic field, *J. Geophys. Res.*, *112*, A10224, doi:10.1029/2007JA012522.

Wang, C.-P., L. R. Lyons, R. A. Wolf, T. Nagai, J. M. Weygand, and A. T. Y. Lui (2009), The plasma sheet $PV^{5/3}$ and nv and associated plasma and energy transport for different convection strengths and AE levels, *J. Geophys. Res.*, *114*, A00D02, doi:10.1029/2008JA013849.

Wang, C.-P., L. R. Lyons, T. Nagai, J. M. Weygand, and A. T. Y. Lui (2010), Evolution of plasma sheet particle content under different interplanetary magnetic field conditions, *J. Geophys. Res.*, *115*, A06210, doi:10.1029/2009JA015028.

Wang, C.-P., M. Gkioulidou, L. R. Lyons, R. A. Wolf, V. Angelopoulos, T. Nagai, J. M. Weygand, and A. T. Y. Lui (2011), Spatial distributions of ions and electrons from the plasma sheet to the inner magnetosphere: Comparisons between THEMIS-Geotail statistical results and the Rice convection model, *J. Geophys. Res.*, *116*, A11216, doi:10.1029/2011JA016809.

Wing, S., J. R. Johnson, P. T. Newell, and C.-I. Meng (2005), Dawn-dusk asymmetries, ion spectra, and sources in the northward interplanetary magnetic field plasma sheet, *J. Geophys. Res.*, *110*, A08205, doi:10.1029/2005JA011086.